electronics

MDPI

Article

Extending OTDR Distance Span by External Front-End Optical Preamplifier

Adriana Lipovac [1,*], Vlatko Lipovac [1], Mirza Hamza [2] and Vedran Batoš [1]

[1] Department of Electrical Engineering and Computing, University of Dubrovnik, 20000 Dubrovnik, Croatia; vlatko.lipovac@unidu.hr (V.L.); vedran.batos@unidu.hr (V.B.)
[2] Department of Telecommunications, Faculty of Electrical Engineering, University of Sarajevo, 71000 Sarajevo, Bosnia and Herzegovina; mhamza@etf.unsa.ba
* Correspondence: adriana.lipovac@unidu.hr

Abstract: Optical time-domain reflectometer (OTDR) is used to characterize fiber optic links by identifying and localizing various refractive and reflective events such as breaks, splices, and connectors, and measuring insertion/return loss and fiber length. Essentially, OTDR inserts a pulsed signal into the fiber, from which a small portion that is commonly referred to as Rayleigh backscatter, is continuously reflected back with appropriate delays of the reflections expressed as the power loss versus distance, by conveniently scaling the time axis. Specifically, for long-distance events visibility and measurement accuracy, the crucial OTDR attribute is dynamic range, which determines how far downstream the fiber can the strongest transmitted optical pulse reach. As many older-generation but still operable OTDR units have insufficient dynamic range to test the far-end of longer fibers, we propose a simple and cost-effective solution to reactivate such an OTDR by inserting a low-noise high-gain optical preamplifier in front of it to lower the noise figure and thereby the noise floor. Accordingly, we developed an appropriate dynamic range and distance span extension model which provided the exemplar prediction values of 30 dB and 75 km, respectively, for the fiber under test at 1550 nm. These values were found to closely match the dynamic range and distance span extensions obtained for the same values of the relevant parameters of interest by the preliminary practical OTDR measurements conducted with the front-end EDFA optical amplifier, relative to the measurements with the OTDR alone. This preliminary verifies that the proposed concept enables a significantly longer distance span than the OTDR alone. We believe that the preliminary results reported here could serve as a hint and a framework for a more comprehensive test strategy in terms of both test diversification and repeating rate, which can be implemented in a network operator environment or professional lab.

Keywords: OTDR; distance span; noise floor; optical amplifier

Citation: Lipovac, A.; Lipovac, V.; Hamza, M.; Batoš, V. Extending OTDR Distance Span by External Front-End Optical Preamplifier. *Electronics* **2021**, *10*, 2275. https://doi.org/10.3390/electronics10182275

Academic Editors: Gennady E. Veseloy, Anton Pljonkin and Lilia Sabantina

Received: 13 May 2021
Accepted: 26 July 2021
Published: 16 September 2021

1. Introduction

Amongst the test equipment needed to install and maintain state-of-the-art fiber optic communication systems, the optical time-domain reflectometer (OTDR) remains the troubleshooting and fault locating tool of choice for fiber characterization in terms of identification and localization of various refractive and reflexive events, e.g., breaks, as well as for measuring attenuation, splice and connector insertion/return losses [1–3].

Moreover, in contrast to legacy OTDRs designed to out-of-service test inactive ("dark") fibers only, the new OTDR generation is equipped with filtered ports, enabling in-service measurements on active fibers carrying live traffic, by generating pulses at 1625 nm or 1650 nm wavelength, which do not belong to the windows used for optical transmission of user traffic [1].

Specifically, concerning the long-distance measurements, especially the far-end events visibility and measurement accuracy, the crucial OTDR attribute is dynamic range, which is the difference between the backscatter level at the front end and the noise floor at the

far end of the fiber. Consequently, the dynamic range determines how far downstream the fiber can the strongest (i.e., of longest duration) transmitted optical pulse reach, also taking into account OTDR span reduction introduced by connectors, splices, and splitters. Consequently, the dynamic range should be about 5 to 8 dB larger than the maximal loss that the OTDR can measure [1,4–8].

On the other hand, looking from the bottom up, the lower boundary determining the OTDR dynamic range is the noise floor value, which is (mostly) where the signal-to-noise ratio (SNR) equals unity, and is observed against the longest pulse width, after the three-minute averaging time [9].

With this regard, still many older-generation OTDR units have insufficient dynamic range to test the far end of long fibers. For example, out of a typical dynamic range of, say, 35 dB, by subtracting attenuations of splices, just about 30 dB remains usable. This implies a considerable reduction of distance span which can be reliably tested with such OTDR units, which reduces their application range and therefore makes them left unused in test tools inventories of network operators [1].

However, in this paper, we introduce a simple and cost-effective solution to reactivate such OTDRs and make them capable of reaching significantly farther along the fiber, by extending their dynamic range. With this regard, for constant laser saturation power level determined by the chosen pulse width, lowering the OTDR noise floor is the only option for widening the dynamic range, and thus extending the distance range. This makes sense, as the OTDR receiver noise figure is anything but small, since it is mostly determined by the large noise figure of the passive optical directional coupler (ODC) [3] the very first block which the returning backscatter passes through before entering the detector.

We inserted a low-noise high-gain optical preamplifier in front of the OTDR, thus making the noise figure of the cascade dominantly determined by the (lower) noise figure of the optical preamplifier, which, according to our preliminary tests in this research-motivating framework of a network operator environment, enabled the OTDR to reach considerably farther along the same fiber under test.

As to our best knowledge, no similar investigation has been reported in public literature, the problem identification could not be reviewed in the standard way by citing detailed achievements and drawbacks of formerly published related solutions, to serve as our motivation for proposing a better approach.

Instead, we consider the other investigations involving dynamic range enhancements (e.g., optimizing its balance with dead zones) complementary rather than mutually exclusive with the proposed model, and therefore, we placed the comments on the related references in a separate Section 4.3. about potential model enhancements "on top of" distance span extension that we proposed in this work.

Accordingly, in Section 2, we present the analysis of all relevant aspects of OTDR measurements, with an accent on dynamic range, noise floor reduction, and distance range extension, whereas in Section 3, we express the preliminary test results, which are discussed in Section 4. Conclusions are summarized in Section 5.

2. Analysis

Essentially, an OTDR inserts a pulsed signal into the fiber, from which a small portion that is commonly referred to as Rayleigh backscatter, is continuously reflected back by irregularities in the optical fiber structure, with the appropriate delays of the reflections expressed as the power loss versus distance, by appropriately scaling the time axis in relation to the speed of light in the fiber determining its refraction index.

Accordingly, an OTDR comprises a microprocessor, a pulse trigger and generator, a laser diode, an optical coupler, a detector, an analog-to-digital converter, and a display, Figure 1.

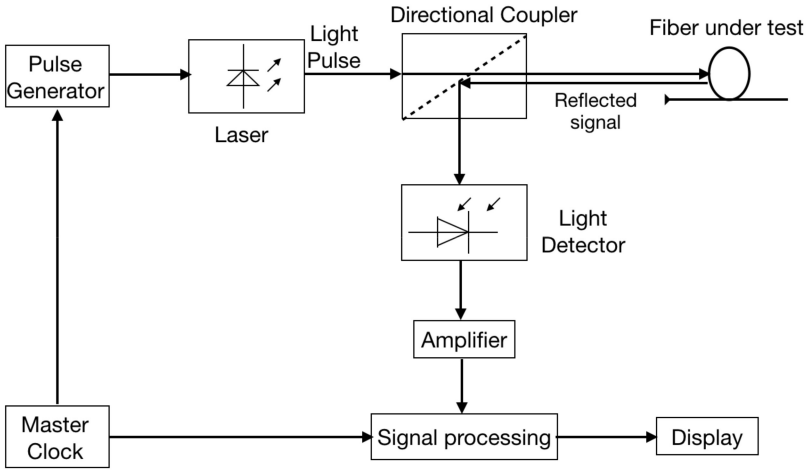

Figure 1. OTDR architecture.

When the test is started, the microprocessor sends a set of instructions to the trigger and generator that tells the laser to send a pulse. The pulses then pass through the directional optical coupler to the OTDR port and into the fiber being tested. In the reverse direction, the ODC channels the reflected signal away from the originating laser and into the detector mostly the avalanche photodiode (APD). Then the signal passes through the analog-to-digital converter to the microprocessor for analysis and display. The processor then averages the data to improve the SNR and displays the points that make up the fiber trace or waveform.

The trace is a collection of tens of thousands of sampling points. Because of the OTDR's limited display resolution, not all of these data points can be displayed, so each point on the screen represents an average of a dozen sampling points.

2.1. Basic OTDR Model

More precisely, when the OTDR transmits the light pulse of power P_0 into the fiber, then the power $P_T(z)$ of the pulse propagating downstream the fiber, is the exponential function of distance z of the observation point from the fiber near-end (OTDR):

$$P_T(z) = P_0 \times 10^{-\alpha \cdot z/10} \quad (1)$$

where $\alpha = \alpha_s + \alpha_a$ is the sum of the scattering and absorption losses expressed in dB/km.

The total scattered power at distance z is:

$$P_s(z) = \alpha'_s \times \Delta z P_T(z) \quad (2)$$

where $\alpha'_s = 0.23 \cdot \alpha_s$ and Δz denote the fiber loss and the light pulse length, respectively.

The latter can be expressed as:

$$\Delta z = w \times v_{gr} = w \times c/n_{gr} \approx w \times c/n \quad (3)$$

where w, v_{gr}, n_{gr}, and c denote the pulse duration, the group velocity in the fiber, the group refractive index (justifiably approximated by the ordinary index n), and the speed of light in vacuum, respectively.

Determined by the fiber numerical aperture, i.e., by limited efficiency of an optical fiber to confine the incident light, only a certain part $S < 1$ of the scattered light travels back to the OTDR (and is being subjected to equal loss, as during forward propagation), and reaches the observation point (that is z apart from the OTDR) with the total backscattered power:

$$P_{BS}(z) = T_s \times S \times \alpha'_s \times \Delta z \times P_0 \times 10^{-2\alpha \cdot z/10} \quad (4)$$

where T_s is the transmission coefficient of the OTDR directional coupler.

So, the maximal backscattered power at the input of the fiber, i.e., at $z = 0$, is:

$$P_{BS}(0) = T_s \times S \times \alpha'_s \times \Delta z \times P_0 \quad (5)$$

Analogously, the backscattering power reflected from the end of the fiber ($z = L$) is:

$$P_{BS}(L) = T_s \times S \times \alpha'_s \times \Delta z \times P_0 \times 10^{-2\alpha \cdot L/10} \quad (6)$$

The signal returning to the OTDR consists of both Rayleigh scattering and Fresnel reflections, where the latter is much stronger than the former. Rayleigh backscattering comes from the natural reflection and absorption of impurities inside the optical fiber. It enables calculating the level of fiber attenuation as a function of distance, which is represented by the constantly falling apart of an OTDR trace. However, Fresnel reflection occurs when the light pulse light hits an abrupt change in refraction index, which causes a strong reflection back, and therefore enables detection of physical events along with the fiber link identifiable by spikes in OTDR trace due to connectors, mechanical splices, bulkheads, fiber breaks or opened connectors (the higher the spike with respect to the backscatter levels, the greater the reflectance). Non-reflective events are caused by fusion splices or bending, and are visible as discrete drops in backscatter level, Figure 2.

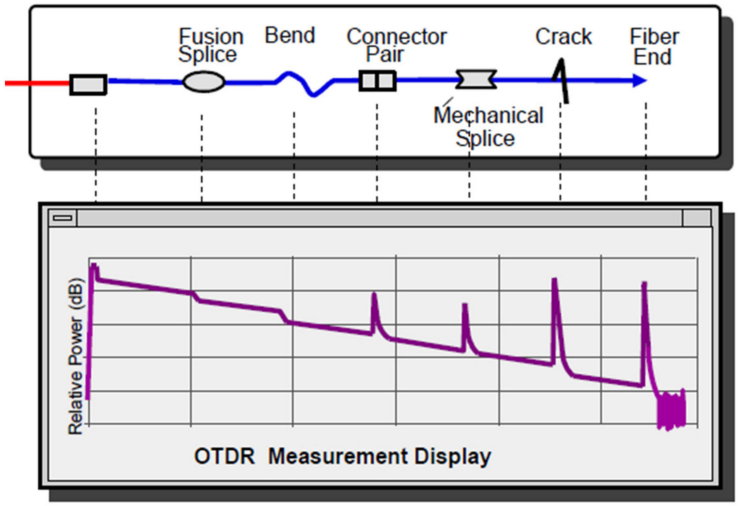

Figure 2. OTDR trace.

In order to apply Equation (5) to estimate the maximal backscattered power at 1550 nm and 1300 nm, we need to adopt some typical parameters' values, such as the ones in Table 1.

Table 1. Typical parameters' values.

Wavelength	1300 nm	1550 nm
$A = \alpha_s + \alpha_a$	0.4 dB/km = 1.092/km	0.2 dB/km = 1.046/km
α'_s	0.074/km	0.036/km
W	1 µs	1 µs
T_s	1	1
S	9.8×10^{-4}	9.8×10^{-4}
$P_{BS}(0)/P_0$	−48.4 dB	−51.5 dB

For example, quite a low backscatter power level $P_{BS}(0)$ being about 50 dB below the incidence power level P_0, is close to the noise floor of the receiver, and is therefore

commonly referred to as Noise Equivalent Power (NEP) [10], so that the SNR must be increased by averaging, which effectively reduces NEP to:

$$NEP_{\text{eff}} = NEP/n^{1/2} \tag{7}$$

where n is the count of averaged samples.

As the OTDR sends light pulses repetitively into the fiber, the responses are computationally averaged, which reduces the receiver noise floor NEP_{eff}, Figure 3.

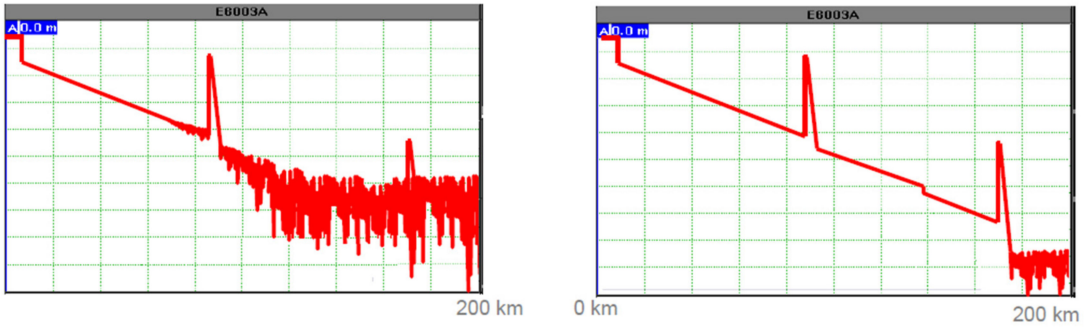

(**a**) (**b**)

Figure 3. OTDR trace. (**a**) after 10 s averaging time, (**b**) after 3 min averaging time.

2.2. OTDR Performance Parameters–Dynamic Range and Distance Span

An OTDR's performance can be accurately evaluated by briefly examining the following key specifications: dynamic range and dead zone caused by the high-return-power Fresnel reflection (mostly from the fiber near-end first connector) that saturates the OTDR detector, disabling detection of events or measuring within that zone of the OTDR trace.

As it was pointed out above, dynamic range is defined as the difference (in dBs) between the maximal backscattered power Equation (5) at the input of the fiber, and the effective noise equivalent power Equation (7):

$$DR\ [\text{dB}] = [P_{\text{BS}}\ (0) - NEP_{\text{eff}}] \tag{8}$$

where the latter is sometimes related to the peak noise floor, implying a 2.2 dB smaller dynamic range than it is with SNR = 1.

Dynamic range depends on the setup parameters' values. The main influences are pulse width, optimization mode, and wavelength.

From a top-down point of view, longer pulses provide larger dynamic range and, consequently, fiber end visibility but also worse event resolution and longer attenuation dead zone, Figure 4.

On the other hand, from the bottom-up perspective, with already chosen pulse width, dynamic range can be increased by lowering NEP_{eff}. A way to do it is averaging, as it is already elaborated above and illustrated in Figure 3, where significant improvements are achieved within the first three minutes of averaging, implying no need for a longer average time.

As it was pointed out above, dynamic range determines the maximal length of fiber that the longest pulse can reach; the larger the dynamic range, the longer the distance. So, if either the loss of a fiber under test is too high, or the dynamic range is insufficient, the far end of the fiber disappears in the noise, whereas in the opposite case, it is visible above the noise floor, and it is possible to detect the break. As connectors, splices, and splitters reduce the maximal fiber length that an OTDR can span, averaging for a longer period and using the proper distance range setup, is the key to increase the maximal measurable distance.

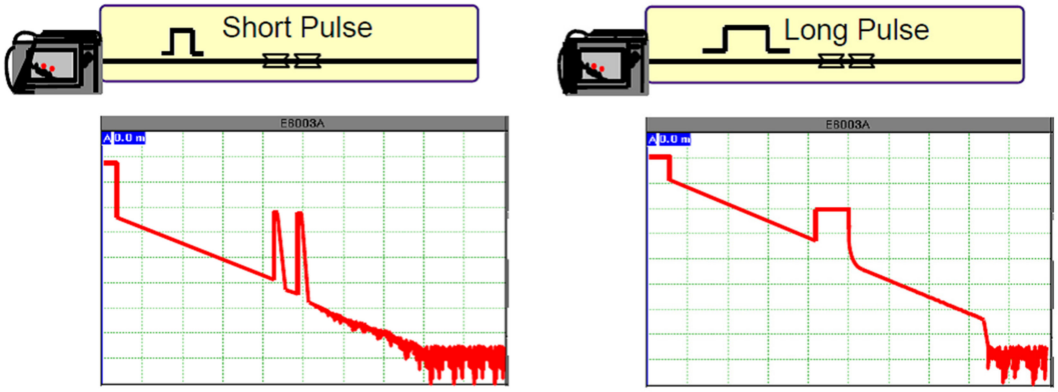

(**a**) (**b**)

Figure 4. OTDR trace. (**a**) with a short pulse for better event resolution; (**b**) with a longer pulse for a longer span.

A good rule of thumb is to choose an OTDR with a dynamic range that enables the trace to remain at least 6 dB and 3 dB above the noise, in order to allow measuring of a 0.1 dB splice and detect a break, respectively. This requires the dynamic range to be at least 5 to 8 dB larger than the total optical transmission system loss [4] to be encountered.

Consequently, a single-mode OTDR with a 35 dB dynamic range has a usable dynamic range of approximately 30 dB. Assuming typical single-mode fiber attenuation of 0.20 dB/km at 1550 nm, and splices every 2 km (loss of 0.1 dB per splice), such OTDR will be able to accurately certify distances of up to 120 km.

Accordingly, subtracting attenuations of all discrete loss events, the maximal distance could be approximately calculated by dividing the rest of the dynamic range of the OTDR by the attenuation (per distance unit) of the fiber [4].

The end of the fiber can be seen as a reflective or non-reflective event, which condition is characterized by the noise after the event indicating the actual fiber end or brake, which may not necessarily be reflective.

2.3. OTDR Receiver Noise Floor Model

As we are interested here in lowering the OTDR noise floor (NEP) to widen the dynamic range, and thus extend the distance span, let us relate NEP to the commonly used receiver inherent noise descriptor—the noise figure, which is generally accepted as a measure of the excess noise that a device itself adds to the incoming noise.

Moreover, as we are to enhance the OTDR receiver by inserting a new front-end block, let us recall that the noise characteristics of a receiver cascade of blocks are commonly modeled by the noise figure.

2.3.1. Noise Floor vs. Noise Figure

Concretely, the noise figure expresses how much larger is the noise power spectral density P_{no} at the receiver output than the input noise power spectral density P_{ni} multiplied by the transmission gain G of the device, assuming shot noise at the input [11]:

$$F = P_{no}/G \times P_{ni} = 1 + NEP_{eff}/G \times P_{ni} \quad (9)$$

From Equation (9), it follows that the noise floor NEP_{eff} is linear with the noise figure F:

$$NEP_{eff} = (F - 1) \times G \times P_{ni} \quad (10)$$

However, the noise figure is rarely given in OTDR technical specifications; rather it is the noise floor that can be found or easily calculated from common OTDR parameters such as its output optical power level and dynamic range.

Nevertheless, due to linear relationship Equation (10), our considerations of reducing the OTDR receiver noise figure are directly applicable to the targeted reduction of its noise floor NEP_{eff} and consequent extension of its dynamic range and, finally, distance span [1].

Furthermore, as can be seen in Figure 1, the OTDR backscatter receiver path includes the ODC and the APD detector. Let us consider the noise contribution (in terms of noise figure) of each of these, and then of the whole cascade.

2.3.2. APD Noise Figure

APD is widely used in test instrumentation, offering NEP lesser than 10^{-15} W/Hz$^{\frac{1}{2}}$ [12,13] determined mostly by shot noise due to stochastic behavior of photons and signal multiplication therefore the name: Poisson noise, which is sometimes also referred to as "gain noise" [11], and described by the excess noise factor ENF [12]. Moreover, a number of other affecters determine the APD noise floor, among them the reverse bias voltage and load. As related to the latter, Johnson noise is caused by the thermal motion of charged particles in a resistive element, and is typically much stronger than the intrinsic shot noise for low bandwidth applications, when the effective noise floor is therefore to the large extent determined by the load resistance.

2.3.3. ODC Noise Figure

On its way to APD, the backscattered signal firstly transverses the ODC, which not only introduces its intrinsic insertion loss between the input and the designated output, but also absorption and backscattering caused by imperfections in the fused region, always creating an excess loss that is a source of excess noise.

Moreover, the noise figure of a passive device is simply equal to its attenuation, implying that the SNR at the ODC output is that much lower than at the input, i.e., that the ODC insertion loss effectively makes it a noise generator whose power is linear with the attenuation [3].

Therefore, insertion loss of an ODC is the important OTDR system design parameter. For a high-quality ODC, both the directionality and the reflection should be typically lower than -55 dB (with optical terminators at unused connector ports) [3].

2.3.4. Noise Figure of Cascaded ODC and APD

Finally, as the OTDR backscatter signal receiver is, in fact, an APD, preceded by the ODC, we recall that, generally, the noise figure $F_{1,2}$ of the cascaded two blocks is to the large extent determined by the noise figure F_1 of the first block (with large gain $G_1 >> 1$) in the series:

$$F_{1,2} = F_1 + (F_2 - 1)/G_1 \approx F_1 \tag{11}$$

The above classic relation describes that the second stage is fed with noise well above the shot noise limit (assuming that the first stage has significant gain). Therefore, the excess noise of the second stage is not very relevant (unless it is very strong), and it does not contribute significantly to the noise figure of the cascade.

However, in the case of the OTDR receiver, not only is the older-generation APD quite noise-rich [1], but the passive front-end ODC with insertion loss A_{DC} (equal to its NF), deteriorates the noise figure of the cascade Equation (11) even further to:

$$F_{\text{OTDR}} = A_{\text{DC}} + (F_{\text{APD}} - 1) \times A_{\text{DC}} = A_{\text{DC}} \times F_{\text{APD}} \tag{12}$$

From Equation (12), it implies that, for the class of older-generation OTDRs represented by the one under test here, we can justifiably consider the OTDR receiver noise figure, and thereby the OTDR noise floor, relatively high.

This motivates the investigation of reducing the OTDR noise floor by inserting a low-noise-figure high-gain optical preamplifier in front of the OTDR through the enhanced branching provided by means of a low-insertion-loss optical circulator (rather than ODC).

This would make the noise figure of the cascade dominantly determined by the (lower) noise figure of the front-end optical amplifier (OA).

2.3.5. Noise Figure of OA with Small-Loss Coupling

While the noise figure of electronic amplifiers is defined around the thermal noise, it is the shot noise that matters here, as the photon energy is far below the thermal one [14–16].

Wide wavelength band, flat gain over a large dynamic gain range, high saturated output power, and low noise are the main features that state-of-the-art erbium-doped fiber amplifiers (EDFA) provide [14–16].

Since the doped fiber of the fiber amplifier and the fiber of the transmission line are generally compatible, high coupling efficiency is feasible. This leads to a low noise figure in the range of 4–6 dB for fiber pre-amplifier(s) used at the far end of a link [17–19], which should provide high gain, often in the range of 30 dB, in order to enable error-free information transport.

On the other hand, optical circulator (OC) is a passive optical component widely used in lightwave communications to separate optical signals traveling in opposite directions over optical fiber, and so, for example, enable bi-directional transmission over a single fiber [3].

OC is based on the nonreciprocal polarization of the optical signal by the Faraday effect. It is a 3-port or a 4-port device as illustrated for the former one in Figure 5a, where "1" denotes the input port, and "2" is the output port. The signal reflected back into port 2 will be redirected (with minimal loss) to port 3, and not to port 1, Figure 5a.

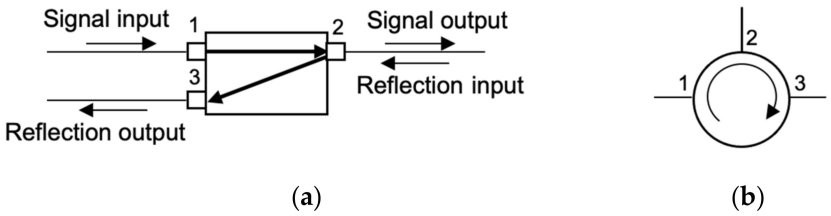

Figure 5. 3-port optical circulator. (**a**) the basic function, (**b**) symbolic presentation.

In OC, light entering any port exits from the next one pointed to by the arrow in the symbolic OC presentation in Figure 5b.

Because of its high isolation of direct from reflected light, and its low insertion loss (of a fraction of dB), OC is used in various optical devices and fiber optic sensors.

Accordingly, as ODC used within the OTDR under test to separate the optical signals of opposite directions, provides a considerable intrinsic insertion loss, in our OTDR preamplifier solution, we used OC as the signal separation front-end, rather than ODC [3,4].

3. OTDR Dynamic Range and Distance Span Extension by Inserting Front-End OA

Let us consider now the noise figure of the cascaded 4-port OC, OA, and OTDR, constituting the test configuration presented in Figure 6.

The OC port 2 is isolated from the adjacent OC port 3, as these are externally interconnected by the OA.

We will first model the dynamic range (and consequent distance span) extension, and then verify the estimated values by the measured ones [20,21].

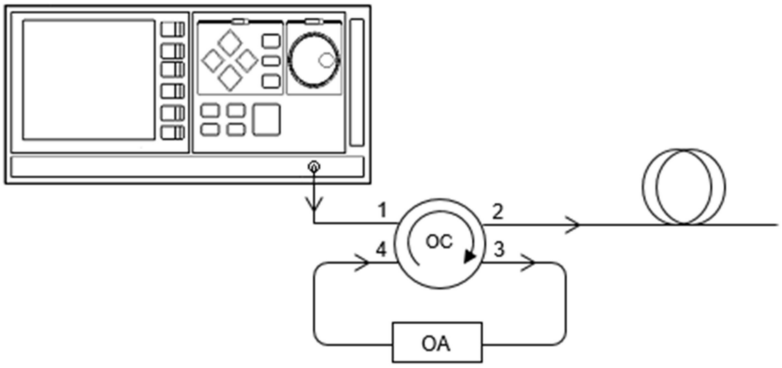

Figure 6. Test configuration: cascaded OC, OA, and OTDR.

3.1. Dynamic Range and Distance Span Extension Prediction Model

From Equation (11), analogously to Equation (12), the noise figure of the cascaded OC and OA is:

$$F_{OC+OA} = A_{OC} \times F_{OA} \tag{13}$$

Furthermore, as $0 < A_{OC} << A_{DC}$, and $1 < F_{OA} << F_{APD}$, from Equation (12) and Equation (13), it implies that:

$$F_{OC+OA} << F_{OTDR} \tag{14}$$

Consequently, taking into account Equation (11), the noise figure of the whole cascade consisting of the 4-port OC, OA, and OTDR, presented in Figure 6, is:

$$F_{OC+OA+OTDR} = F_{OC+OA} + (F_{OTDR} - 1)/G_{OC+OA} \approx F_{OC+OA} = A_{OC} \times F_{OA} \tag{15}$$

where we considered $G_{OC+OA} \approx G_{OA} >> A_{OC}$ (quite justifiably as G_{OA} is of the order of 10^3 and thereby much larger than the OC insertion loss A_{OC}).

Thereby, recalling Equation (12), from Equation (15) it is obvious that:

$$F_{OC+OA+OTDR} \approx A_{OC} \cdot F_{OA} << F_{OTDR} = A_{DC} \times F_{APD} \tag{16}$$

i.e., that introducing the OTDR front-end optical pre-amplifier significantly reduces the noise figure, and thereby widens the dynamic range.

Coming out of Equation (10), reducing the noise figure, i.e., the SNR degradation by the OTDR receiver chain adding its own inherent noise, would reduce the OTDR noise floor – the lower bound of the OTDR dynamic range (where SNR=1), and thus widen the dynamic range for ΔDR as it implies from Equation (8):

$$\Delta DR = [P_{BS}(0) - NEP_{OC+OA+OTDR}] - [P_{BS}(0) - NEP_{OTDR}] = NEP_{OTDR} - NEP_{OC+OA+OTDR} \tag{17}$$

From Equation (10), it is obvious that, for certain input noise power P_{ni}, the noise floor NEP_{OTDR} for the OTDR alone is:

$$NEP_{OTDR} = (F_{OTDR} - 1) \times G_{OTDR} \times P_{ni} \tag{18}$$

whereas for the cascaded OC, OA, and OTDR, it is:

$$NEP_{OC+OA+OTDR} \approx NEP_{OA} = (F_{OA} - 1) \times G_{OA} \times P_{ni} \tag{19}$$

So, the noise floor reduction (and consequent dynamic range extension) as a benefit of inserting the preamplifier, can be obtained if we divide Equation (18) by Equation (19), or perform the subtraction in dB units.

However, the OTDR noise figure F_{OTDR} (specifically its constituents A_{DC} and F_{APD}) and gain G_{OTDR} are rarely given in technical specifications, whereas its noise floor NEP_{OTDR}

(in dB units) can be easily estimated by subtracting the specified dynamic range from the maximal output optical power level.

On the contrary, the OA noise figure F_{OA} and gain G_{OA} is always specified, whereas it is not the case with the OA noise floor NEP_{OA}.

Considering the OTDR alone, the SNR at its receiver output is:

$$P_{sOTDR}/P_{nOTDR} = G_{OTDR} \cdot S_{inp}/NEP_{OTDR} = 1 \quad (20)$$

where S_{inp} is the input signal power, and introducing the optical pre-amplifier implies the following SNR at the OTDR receiver output:

$$P_{sOA+OTDR}/P_{nOA+OTDR} = G_{OA} \cdot \times G_{OTDR} \cdot \times S_{inp}/(G_{OTDR} \cdot \times NEP_{OA} + NEP_{OTDR}) \quad (21)$$

Furthermore, considering Equations (20) and (21) simplifies to:

$$P_{sOA+OTDR}/P_{nOA+OTDR} = G_{OA} \cdot \times NEP_{OTDR}/(G_{OTDR} \cdot \times NEP_{OA} + NEP_{OTDR}) \quad (22)$$

The noise floor reduction (and consequent dynamic range extension ΔDR) as a result of inserting a preamplifier is obtained dividing Equation (22) by Equation (20) as it follows:

$$\Delta DR = (P_{sOA+OTDR}/P_{nOA+OTDR})/1 = G_{OA} \cdot \times NEP_{OTDR}/(G_{OTDR} \cdot \times NEP_{OA} + NEP_{OTDR}) \quad (23)$$

In dB units, Equation (23) can be expressed as:

$$\Delta DR[\text{dB}] = 10 \log \Delta DR = G_{OA}[\text{dB}] + NEP_{OTDR}[\text{dBm}] - 10 \log(G_{OTDR} \cdot NEP_{OA} + NEP_{OTDR}) \quad (24)$$

The dynamic range extension Equation (24) implies the following distance range extension:

$$\Delta L_{OA+OTDR}\ [\text{km}] = \Delta DR[\text{dB}]/2 \times \alpha[\text{dB/km}] \quad (25)$$

3.2. Dynamic Range and Distance Span Extension Prediction Values

Let us make an exemplar prediction of dynamic range extension and distance span extension by means of Equations (23) and (24), as well as Equation (25), respectively, adopting common values for the relevant parameters of interest:

By conducting measurement, we found the OTDR noise floor NEP_{OTDR} value to be close to -50 dBm, which corresponds to NEP_{OTDR} = 10 nW on the linear scale.

Furthermore, let us suppose the EDFA preamplifier gain G_{OA} of 30 dB and the noise figure F_{OA} of 6 dB [22]. The latter implies the OA noise floor spectral density value of 10^{-5} nW/Hz$^{1/2}$ [11], so that the noise bandwidth of 0.2 MHz (in accordance with the pulse duration of 5 μs), results with:

$$NEP_{OA} = 10^{-5}\ \text{nW/Hz}^{1/2} \cdot \times (2 \cdot 10^5)^{\frac{1}{2}} \times \text{Hz}^{1/2} = 447 \times 10^{-5}\ \text{nW} \quad (26)$$

On the other hand, we consider the OTDR receiver GaAs APD gain to range between 10 and 40 dB [13], and choose to adopt the pessimistic value of G_{OTDR} = 10 dB.

Furthermore, substituting the above exemplar values into Equations (23) and (24) provides the predicted dynamic range extension value of $\Delta DR \approx 996$ and $\Delta DR \approx 30$ dB, respectively.

Finally, substituting the latter value into Equation (25), and adopting α = 0.2 dB/km for the fiber attenuation at 1550 nm, we estimate the distance range extension of 75 km.

4. Preliminary Test Results

4.1. Test System

We used the HP 8147A optical time-domain reflectometer, designed for fiber characterization that network operators conduct during installation and field maintenance of their optical transmission systems, Figure 7.

Figure 7. OTDR under test.

The OTDR contained the plug-in optical interface module for both 1310 nm and 1550 nm optical windows, and was connected in the test configuration cascade with OC and OA according to Figure 6.

After selecting fiber type (single-mode in our case), wavelength, and index of refraction, the main parameters to set up were: maximal distance range (i.e., fiber length), pulse width, and acquisition time.

As our distance span extension model is centered around the dynamic range, according to the considerations in Section 2.2. that longer pulses reach farther along the fiber, we selected 5 µs as quite sufficient for the fiber that we tested.

Having set the pulse width, the OTDR automatically selected the coupled distance range and standard acquisition time values, optimized for the particular fiber under test.

Distance accuracy can be enhanced by proper calibration of the entire OA-OTDR test system, but this requires cost demanding additional equipment [23,24]. Unfortunately, it is not available at this point of our research, so our preliminary test results are aimed to just verify the proposed concept, rather than present any firm reference value with this regard.

The follow-up high-accuracy measurements can be repeated as many times as needed for various tests of this kind. So, for example, the OA transmission characteristics ripple, if significant, must be taken into account, as considering transfer function a Fourier series, any sinusoidal ripple in the frequency/wavelength domain, is equivalent to a pulse in the time domain (whose delay is determined by the frequency of the corresponding sinusoid) [25]. Consequently, a "wavy" OA transfer characteristics could introduce ghost pulses (i.e., events) into the OTDR trace.

4.2. Results

The exemplar preliminary test traces of the OTDR alone, and of the OTDR with the front-end OA, are presented in Figure 8a,b, respectively.

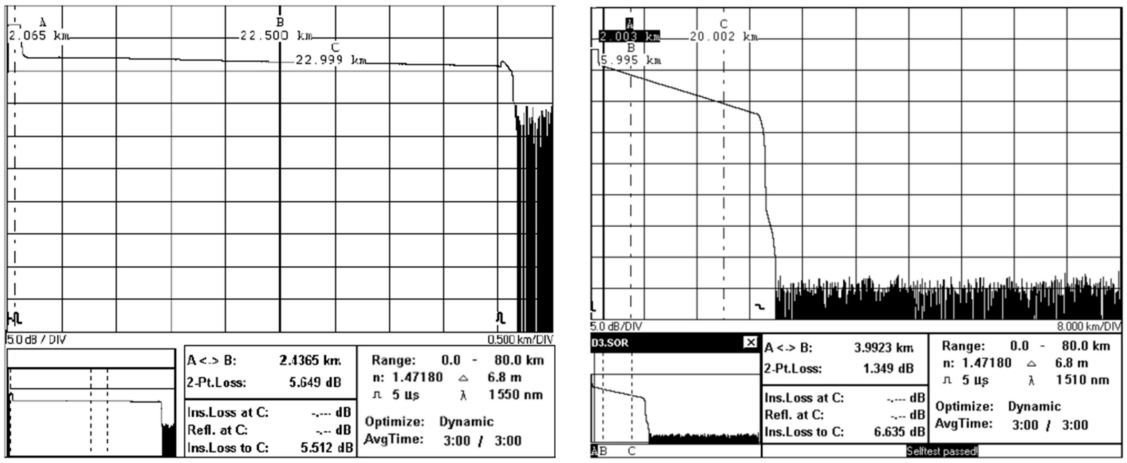

(**a**) (**b**)

Figure 8. Preliminary OTDR test traces; (**a**) OTDR alone, (**b**) OTDR with the front-end OA.

As it can be seen, the significant difference is evident between the noise floor values in these cases, with the dynamic range enhancement of about 30 dB, which conforms to the predicted value obtained from Equation (24), and consequently verifies the distance span extension of 75 km estimated by Equation (25) as well.

Testing in other optical windows will not be any different, except requiring a more expensive PDFA preamplifier at 1310 nm, thus questioning the profitability of the solution.

We believe that the preliminary results reported here could serve as a hint and a framework for a more comprehensive test strategy in terms of both test diversification (with more fiber links with various events), and repeating rate, which can be implemented in a network operator environment or professional lab.

4.3. Discussion and Potential Model Enhancements

The initial motivation for the proposed model is now planned to stretch beyond just reactivating the older-generation OTDR units, to include other potential enhancements, such as coding, advanced signal processing, trace post-processing, interaction with existing active devices of the fiber optic link, as well as in-service testing.

More specifically, as the here proposed OTDR enhancement targets only distance span extension, the far-end events which (this way) have become visible by introducing the OA front-end, will preserve the resolution of the former OTDR-only far-end ones, whereas, for the shorter distances, no preamplifier should be used.

However, systematic mitigating the impact of OTDR attenuation and event dead zones, specifically once having extended the distance range by the optical preamplifier, deserves to be considered, too. For given receiver bandwidth, a possible solution is to reduce the OTDR noise floor by using simplex codes (scs) [26], which can be extended to the general noise model in the coded OTDR combining the scs with the complementary correlation codes to achieve higher gains [27].

Furthermore, the OTDR dynamic range can be extended by some more advanced signal processing techniques to lower the noise floor of backscattering-based systems in general, such as translation-invariant wavelet thresholding (TIWT), and lifting wavelet transform-modified particle swarm optimization (LWT-MPSO) [28].

Moreover, advanced OTDR trace postprocessing algorithms such as vector indexing, are also of interest for event detection, location, and spatial resolution [29].

Finally, in an OTDR based sensor system, using EDFA has created an experimental knowledge base regarding gain, insertion loss, and pumping configurations, which would be worth merging with the analytical model derived here [30–34].

As the proposed dynamic range (and thereby distance span) extension is done by the very “ground-floor” physical layer action - introduction of the front-end OA, the above-

mentioned enhancements could be added "on top of" the proposed model, rather than replace it.

5. Conclusions

Many older-generation OTDR units have insufficient dynamic range to test the far-end of longer fibers. A simple and cost-effective solution for re-activation of these useful and costly devices in installation and maintenance of state-of-the-art fiber-optic links, is shown here to be the introduction of a low-noise high-gain optical preamplifier in front of the OTDR, to effectively reduce its noise floor, as, by this way, the noise figure of the cascade becomes dominantly determined by the front-end optical amplifier.

According to our preliminary tests, this enabled the OTDR to significantly enhance its dynamic range and consequently distance span, by almost 30 dB and 75 km, respectively.

This work was aimed to discover, model, verify and quantify the potential of the proposed OTDR distance span extension, and thereby pave the way to according R&D and field tests taking into account design and deployment issues as well, and using sophisticated hardware and industry-standard software simulation tools.

We believe that the preliminary results reported here could be a hint for a more comprehensive test strategy in terms of both diversification and repeating rate.

Author Contributions: Conceptualization, A.L. and V.L.; methodology, A.L.; software, A.L. and M.H.; validation, A.L., V.L. and M.H.; formal analysis, A.L and V.L.; investigation, A.L.; resources, A.L. and M.H.; data curation, A.L. and M.H.; writing—original draft preparation, A.L.; writing—review and editing, V.L.; visualization, M.H.; supervision, V.B.; project administration, V.B.; funding acquisition, V.L. and V.B. All authors have read and agreed to the published version of the manuscript.

Funding: This research leading to the published results was supported by the Ministry of Civil Affairs of Bosnia and Herzegovina, under Grant No. 02-7142/20.

Institutional Review Board Statement: Not applicable.

Informed Consent Statement: Not applicable.

Data Availability Statement: Not applicable.

Conflicts of Interest: The authors declare no conflict of interest.

References

1. Lipovac, A. Practical Enhancement of Fiber Installation and Maintenance Test Tools-Example of Extending OTDR Distance Range by Optical Preamplifier. In Proceedings of the European Lasers, Photonics and Optics Technologies Summit, Paris, France, 22 September 2020.
2. Winzer, P.J.; Neilson, D.T.; Chraplyvy, A.R. Fiber-optic transmission and networking: The previous 20 and the next 20 years. *Opt. Express* **2018**, *26*, 24190–24239. [CrossRef] [PubMed]
3. Hui, R. Passive optical components. In *Introduction to Fiber-Optic Communications*, 1st ed.; Academic Press: Cambridge, MA, USA, 2020; pp. 209–297.
4. Hui, R.; O'Sullivan, M. Characterization of Optical Devices. In *Fiber Optic Measurement Techniques*, 1st ed.; Academic Press: Cambridge, MA, USA, 2009; pp. 259–363.
5. Lu, X.; Soto, M.A.; Thévenaz, L. Temperature-strain discrimination in distributed optical fiber sensing using phase-sensitive optical time-domain reflectometry. *Opt. Express* **2017**, *25*, 16059–16071. [CrossRef] [PubMed]
6. Alekseev, A.E.; Vdovenko, V.S.; Gorshkov, B.G.; Potapov, V.T.; Simikin, D.E. Fading reduction in a phase optical time-domain reflectometer with multimode sensitive fiber. *Laser Phys.* **2016**, *26*, 95–101. [CrossRef]
7. Hartog, A.H. Frequency-Scanned Optical Time Domain Reflectometry. US Patent 7859654B2, 17 July 2008.
8. Lu, X.; Soto, M.A.; Thévenaz, L. Optimal detection bandwidth for phase-sensitive optical time-domain reflectometry. In Proceedings of the Sixth European Workshop on Optical Fibre Sensors EWOFS'2016, Limerick, Ireland, 31 May 2016; pp. 374–377.
9. Agilent Technologies. Optical Time Domain Reflectometers; Pocket Guide. 2001. Available online: http://literature.cdn.keysight.com/litweb/pdf/E6000-91017.pdf (accessed on 1 May 2021).
10. Mackowiak, V.; Peupelmann, J.; Ma, Y.; Gorges, A. *NEP–Noise Equivalent Power*; Thorlabs, Inc.: Dachau, Germany, 2015; pp. 1–5.
11. Memis, O.G.; Katsnelson, A.; Kong, S.C.; Mohseni, H.; Yan, M.; Zhang, S.; Hossain, T.; Jin, N.; Adesida, I. Sub-Poissonian shot noise of a high internal gain injection photon detector. *Opt. Express* **2008**, *16*, 12701–12706. [CrossRef] [PubMed]
12. Lau, K.S.; Tan, C.H.; Ng, B.K.; Li, K.F.; Tozer, R.C.; David, J.P.; Rees, G.J. Excess noise measurement in avalanche photodiodes using a transimpedance amplifier front-end. *Meas. Sci. Technol.* **2006**, *17*, 1941–1945. [CrossRef]

13. Huntington, A. *Sensitivity Analysis of APD Photoreceivers*; VoxtelOpto, Voxtel Inc.: Beaverton, OR, USA, 2016; pp. 1–39.
14. Olshansky, R. Noise figure for erbium-doped optical fiber amplifiers. *Electron. Lett.* **1988**, *24*, 1363–1365. [CrossRef]
15. Haus, H.A. The noise figure of optical amplifiers. *IEEE Photonics Technol. Lett.* **1998**, *10*, 1602–1604. [CrossRef]
16. Desurvire, E. Comments on 'The Noise Figure of Optical Amplifiers'. *IEEE Photonics Technol. Lett.* **1999**, *11*, 620–621. [CrossRef]
17. Abedin, K.S.; Taunay, T.F.; Fishteyn, M.; Yan, M.F.; Zhu, B.; Fini, J.M.; Monberg, E.M.; Dimarcello, F.V.; Wisk, P.W. Amplification and noise properties of an erbium-doped multicore fiber amplifier. *Opt. Express* **2011**, *19*, 16715–16721. [CrossRef] [PubMed]
18. Chen, H.; Jin, C.; Huang, B.; Fontaine, N.K.; Ryf, R.; Shang, K.; Grégoire, N.; Morency, S.; Essiambre, R.J.; Li, G.; et al. Integrated cladding-pumped multicore few-mode erbium-doped fiber amplifier for space-division-multiplexed communications. *Nat. Photonics* **2016**, *10*, 529–533. [CrossRef]
19. Desurvire, E. *Erbium-Doped Fiber Amplifiers: Principles and Applications*, 1st ed.; John Wiley & Sons: New York, NY, USA, 1994; p. 770.
20. Pedersen, B.; Dakss, M.L.; Thompson, B.A.; Miniscalco, W.J.; Wei, T.; Andrews, L.J. Experimental and theoretical analysis of efficient erbium-doped fiber power amplifiers. *IEEE Photonics Technol. Lett.* **1991**, *3*, 1085–1087. [CrossRef]
21. Giles, C.R.; Desurvire, E. Modeling erbium-doped fiber amplifiers. *J. Lightwave Technol.* **1991**, *9*, 271–283. [CrossRef]
22. Available online: https://nuphoton.com/product-category/fiber-amplifiers/erbium-doped-fiber-amplifiers/ (accessed on 1 May 2021).
23. Larson, D.R.; Paulter, N.G.; Blaney, K.C. Characterization and Calibration of an Optical Time Domain Reflectometer Calibrator. In Proceedings of the National Conference of Standards Laboratories International Workshop and Symposium, Nashville, TN, USA, 7 August 2006.
24. Larson, D.R.; Paulter, N.G.; Blaney, K.C. Calibration of Optical Time-Domain Reflectometers (OTDR's); Technical Report Number: NIST Technical Note 1475. 2006. Available online: https://nvlpubs.nist.gov/nistpubs/Legacy/TN/nbstechnicalnote1475.pdf. (accessed on 1 May 2021).
25. Sunde, E.D. Theoretical fundamentals of pulse transmission—II. *Bell Syst. Tech. J.* **1954**, *33*, 987–1010. [CrossRef]
26. Lee, D.; Yoon, H.; Kim, P.; Park, J.; Park, N. Optimization of SNR Improvement in the Noncoherent OTDR Based on Simplex Codes. *J. Lightwave Technol.* **2006**, *24*, 322–328.
27. Naseem, A.; Mehmood, H.; Muhammad, S.S.; Abbas, S.A. Composite Coding Scheme for OTDR SNR Enhancement. In Proceedings of the Con TEL, Graz, Austria, 2 June 2011.
28. Tangudu, R.; Sahu, P.K. Dynamic Range Improvement of Backscattered Optical Signals using Signal Processing Techniques. In Proceedings of the IEEE Applied Signal Processing Conference (ASPCON), Kolkata, India, 7–9 October 2020.
29. Usama, M.; Muhammad, S.S. Vector Indexing Algorithm for Post Processing of OTDR Data. In Proceedings of the 2013 18th European Conference on Network and Optical Communications & 2013 8th Conference on Optical Cabling and Infrastructure (NOC-OC&I), Graz, Austria, 10–12 July 2013.
30. Lee, H.H.; Nam, Y.H.; Lee, D.; Chung, H.S.; Kim, K. Demonstration of a Low-Cost 1625-nm OTDR Monitoring for 350-km WDM Networks With Semiconductor Optical Amplifiers. *IEEE Photonics Technol. Lett.* **2005**, *17*, 852–854. [CrossRef]
31. Nascimento, J.F.; Cipriano, E.A.; Martins-Filho, J.F.; Guimarães, J.; da Silva, M.J. Characterization of an Amplified OTDR Fiber-optic Multipoint Sensor System. In Proceedings of the International Microwave and Optoelectronics Conference (IMOC 2011), Natal, Brazil, 8 October 2011.
32. Pljonkin, A. Vulnerability of the Synchronization Process in the Quantum Key Distribution System. *Int. J. Cloud Appl. Comput.* **2019**, *9*, 1–10. [CrossRef]
33. Pljonkin, A.; Rumyantsev, K. Quantum-cryptographic network. In Proceedings of the IEEE East-West Design & Test Symposium (EWDTS), Yerevan, Armenia, 14 October 2016; pp. 1–4.
34. Pljonkin, A.; Petrov, D.; Sabantina, L.; Dakhkilgova, K. Nonclassical Attack on a Quantum Key Distribution System. *Entropy* **2021**, *23*, 509. [CrossRef] [PubMed]